Transverse-Stress Fiber Bragg Grating Sensor With High Spatial Resolution and Temperature Stability

R. Joseph Espejo and Shellee D. Dyer

***Abstract*—We demonstrate a new method for measuring transverse stress with 10.2-μm spatial resolution in a fiber Bragg grating sensor, without the use of polarization-maintaining fiber, by combining a four-state polarization analysis with a layer-peeling algorithm. Measurements of the externally induced birefringence agree well with predicted values. We also demonstrate that our measurement is insensitive to temperature changes and spatial gradients, making it ideal for nonisothermal applications.**

***Index Terms*—Fiber Bragg gratings (FBGs), fiber-optic sensors, layer peeling, low-coherence interferometry (LCI), transverse-strain sensors.**

I. Introduction

OVER THE past ten years, fiber Bragg gratings (FBGs) have come to play an important role in passive strain and stress detection. In the simplest form, they are used as optical strain gauges. These devices are either attached to or imbedded in the host material that they are monitoring. As the host experiences strain, so does the optical fiber, which changes the center wavelength of the reflected spectrum. The reflection spectrum is then monitored for shifts in wavelength, indicating a state of strain. The complete state of stress of the host material can be measured by embedding several of these strain gauge sensors in the host in orthogonal directions. This level of complexity can be difficult to implement, and the presence of a large number of sensors may weaken the host [1]. The complete state of stress can be measured with a single FBG, if a polarization-sensitive measurement is used. The FBG can be written in polarization-maintaining (PM) fiber so that the wavelength along the two orthogonal polarization eigenstates can be monitored, giving information about the transverse strain [2], [3]. While measurement of longitudinal stress have no polarization requirements, measurements of transverse stress usually require PM fiber and detection making it difficult to interrogate existing non-PM sensors.

Ambiguities arise when strains occur on scales smaller then the sensor's length, causing an uncertainty for inhomogeneous host materials such as composites. These sensors, therefore, must assume a constant stain across the entire length of the FBG, typically several millimeters, and are, therefore, limited to large-scale strain measurement.

Recently, there has been success in measuring environmental stress on scales smaller than length of the FBG by detecting changes in the refractive index within the FBG [4]–[6]. These typically use an interferometric measurement of the FBG along with an inverse-scattering method such as layer-peeling or genetic algorithms.

Manuscript received October 13, 2006.

The authors are with the National Institute of Standards and Technology, Boulder, CO 80305 USA (e-mail: RJEspejo@gmail.com; sdyer@boulder.nist.gov).

Digital Object Identifier 10.1109/JLT.2007.897718

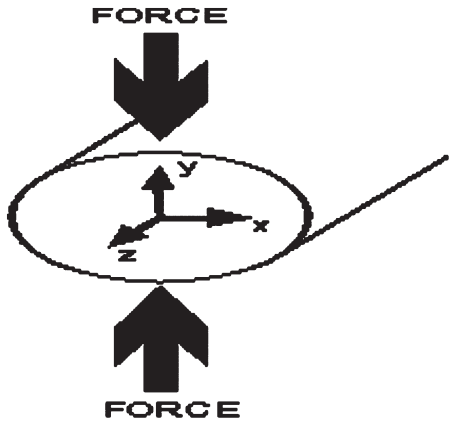

Fig. 1. Schematic showing the defined coordinate system. Force is applied in the y-direction. The fiber core lies along the z-axis. The force causes compression in the y-direction and elongation in the x-direction (exaggerated in the drawing).

In this paper, we present a new method for interrogating a conventional FBG strain sensor that yields measurements of the longitudinal and transverse stress with high spatial resolution. The FBG is written in standard telecom single-mode fiber. Polarization information is obtained through a four-state polarization analysis, so the system requires no expensive PM fiber or devices. This makes it low in cost and applicable to existing sensor systems. Measurements are performed with both time-domain low-coherence interferometry (LCI) and optical frequency-domain reflectometry (OFDR) to demonstrate the flexibility of the four-state method. Our method also shows insensitivity to thermal effects, which is typically a limitation of most FBG strain sensors.

II. Determining the Birefringence

The directional stress in the fiber caused by external transverse strain creates a localized birefringence in the region of strain. To determine the magnitude and relative direction of this birefringence, a polarization-sensitive method is used.

A. Stress in Fibers

When the FBG is transversely compressed, as in Fig. 1, stress in the direction of the applied force σ_y is negative due to compression. Stresses in the two orthogonal directions, σ_x

and σ_z, are positive. When the stress region is longer than the diameter of the fiber, the stresses in the axial direction σ_z cancel, leaving only σ_x and σ_y. In order to simplify the model of fiber stresses, we limit ourselves to this case so that axial elongations that would locally modify the grating's pitch are minimized. For a given compressive force, these stresses are expressed in the Hertz equations [3]

$$\begin{aligned}\sigma_x &= \frac{2F}{\pi DL}\\ \sigma_y &= -\frac{6F}{\pi DL}\\ \sigma_z &= 0\end{aligned} \tag{1}$$

where D is the fiber diameter, F is the applied force, and L is the length of the region under stress.

The applied stress causes an anisotropic change in the effective refractive index n_{eff}, which is given by [2] as

$$\begin{aligned}\delta n_x &= -\frac{n_o^3}{2E}\big([p_{11}(1+\nu)(1-\nu) - p_{12}(1+\nu)\nu]\,\sigma_x \\ &\qquad + [p_{12}(1+\nu)(1-\nu) - p_{11}(1+\nu)\nu]\,\sigma_y\big)\\ &= C_1\sigma_x + C_2\sigma_y\\ \delta n_y &= -\frac{n_o^3}{2E}\big([p_{11}(1+\nu)(1-\nu) - p_{12}(1+\nu)\nu]\,\sigma_y \\ &\qquad + [p_{12}(1+\nu)(1-\nu) - p_{11}(1+\nu)\nu]\,\sigma_x\big)\\ &= C_2\sigma_x + C_1\sigma_y\end{aligned} \tag{2}$$

where δn_x and δn_y are the effective indexes in the x- and y-directions. For the physical parameters of the fiber, we use $n_o = 1.47$ for the refractive index in the unstressed fiber core, $\nu = 0.17$ for the Poisson ratio, and $E = 7.3 \times 10^{10}$ Pa for the Young's Modulus; $p_{11} = 0.113$ and $p_{12} = 0.252$ are the strain-optic coefficients. The constants $C_1 = -1.297 \times 10^{-6}$ mm$^2 \cdot N^{-1}$ and $C_1 = -4.835 \times 10^{-6}$ mm$^2 \cdot N^{-1}$ are defined as the stress-optic coefficients [2], [3]. The refractive index in the x- and y-directions is then given by $n_x = n_o + \delta n_x$ and $n_y = n_o + \delta n_y$, with birefringence

$$\Delta n = \delta n_y - \delta n_x. \tag{3}$$

B. FBG Index Reconstruction

To determine the stress in the FBG with high resolution, we measure the physical refractive-index structure of the FBG, specifically the FBG's effective index. This is accomplished through the application of an inverse-scattering algorithm known as layer peeling to the measured complex reflection spectrum of the FBG. The complex reflection spectrum can be measured by any phase-sensitive reflectometry technique, such as LCI or OFDR, as are described in Section III. A layer-peeling algorithm is then applied to the calculated complex spectrum to determine the complex coupling coefficient in the FBG $q(z)$ [7].

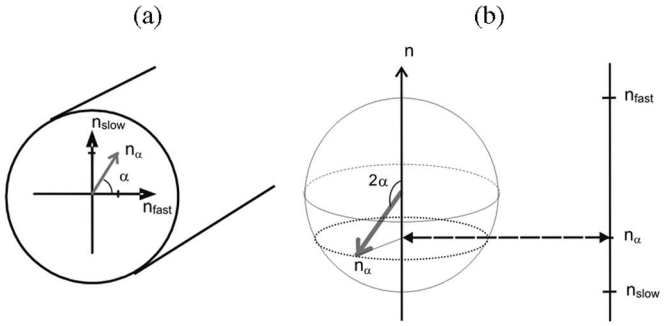

Fig. 2. (a) Polarization-state propagating through the fiber at angle α, with respect to the eigenaxis, will see an effective index n_α. (b) Polarization-state expressed on a modified Poincaré sphere. The eigenaxes are mapped to the axis defined by the orthogonal linear states, labeled $\mathbf{n}$. Refractive index as a function of angle α is then mapped as a projection on to this axis.

The phase of the calculated coupling coefficient can be related to n_{eff} by

$$\arg\left(q(z)\right) = \theta(z) - \frac{2\eta}{\lambda_B}\int_0^z n_{\text{eff}}(z')dz' \tag{4}$$

where $\arg(q(z))$ is the vector phase angle of the coupling coefficient. In order to calculate n_{eff}, we assume that the spatial grating phase $\Theta(z)$ is constant. This assumption requires that all phase changes in the FBG phase are from variations in the refractive index and not a physically varying grating pitch. With this assumption, n_{eff} can be found by differentiating $\arg(q(z))$

$$n_{\text{eff}}(z) = \frac{\lambda_B}{2\eta}\left(\frac{1}{\Lambda_B} - \frac{1}{\Lambda_{\text{eff}}(z)}\right) \tag{5}$$

where λ_B is the Bragg wavelength, Λ_B is the Bragg period, η is the fraction of the modal power in the core of the fiber, and the effective grating period Λ_{eff} is determined from

$$\Lambda_{\text{eff}}(z) = \Lambda_B\left(1 + \frac{\Lambda_B}{2\pi}\frac{d}{dz}\arg\left(q(z)\right)\right)^{-1}. \tag{6}$$

A four-state analysis is then used to find $\Delta n(z)$ from these measurements of $n_{\text{eff}}(z)$.

C. Four-State Analysis

The four-state algorithm is a powerful yet simple tool for gathering polarization information from a system that does not have a PM ability. The algorithm was originally developed for measuring polarization-dependent loss (PDL) and polarization-mode dispersion in optical fibers and components and is also used to measure the polarization-dependent wavelength shift (PDW) in FBGs [8]–[10]. In this paper, we follow closely the method presented by the study in [10], drawing on the relationship between PDW and the polarization-dependent effective index.

The birefringence induced by transverse compression is directional, with the effective index having orthogonal eigenstates in the x- and y-directions, as in Fig. 2(a). If we assume linear

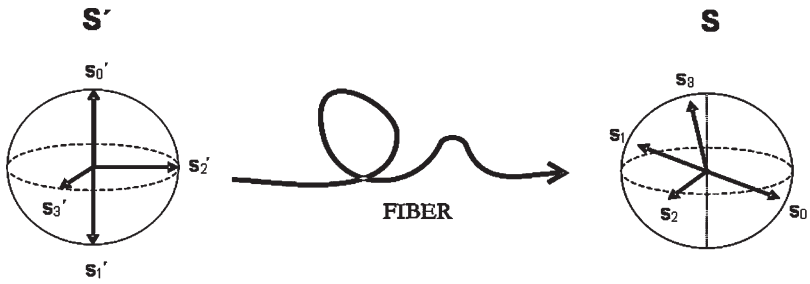

Fig. 3. Schematic showing a length of fiber transforming the collection of states $\mathbf{S}'$ into arbitrary states $\mathbf{S}$. The four launch states maintain their orientation with respect to each other as they propagate through the fiber.

birefringence in the FBG, the effective index seen by the polarization-state will vary sinusoidally with the angle α as the polarization-state moves between the two eigenaxes. The cross states, $\pm 45^\circ$, right-hand and left-hand circular, all occur midway between the two linear eigenstates at $\alpha = 45^\circ$ and should, therefore, have the same effective index. The value of the cross-states is the average of the effective index of the two eigenstates.

To facilitate the four-state calculation, we plot the measured $n_{\rm eff}$ as a function of polarization-state in modified Poincaré coordinates. In these coordinates, the local birefringence in the FBG Δn is plotted as the radial coordinate, which defines the surface of our modified Poincaré sphere. The polarization coordinate axes remain the same, except that the sphere is rotated so the linear states are at the poles. Using this convention, the two orthogonal eigenaxes, $n_{\rm fast}$ and $n_{\rm slow}$, are mapped to the two linear states at the poles of the sphere. Each measurement of $n_{\rm eff}$ is the projection of the polarization vector at the grating to the linear-state polar axis of the Poincaré sphere, labeled $\mathbf{n}$ in Fig. 2(b).

Four states are needed to define the Δn surface. The four states must form a Mueller set: Three lie on a great circle on the sphere separated by 90° in Poincaré coordinates, and the fourth is on the axis of this great circle. Two of these states form an orthogonal pair. For convenience, we chose $\{s_0', s_1', s_2', s_3'\} = \{0^\circ, 90^\circ, +45^\circ,$ right-hand circular$\}$ for the input states in standard coordinates.

In non-PM fiber, a launched polarization-state $\mathbf{S}'$ can evolve in to another arbitrary polarization-state $\mathbf{S}$, as it travels through the fiber to the FBG. However, in the absence of PDL and depolarization, several distinct launch states will maintain their orientation relative to one another on the Poincaré sphere, as shown in Fig. 3. This is because the states all see the same birefringent effects in the fiber and, thus, undergo the same unitary transformation. The four-state analysis uses this preservation of the relative orientation of states in its calculation: The refractive index is measured at four specific polarization launch states, which are then combined to calculate Δn.

To calculate Δn, which is the local diameter of the sphere, we define (7), (8), and (9). The equatorial value of the refractive index is given by

$$\bar{n} = \frac{n_{s0} + n_{s1}}{2} \tag{7}$$

where $n_{\rm s0}$ and $n_{\rm s1}$ are the measured refractive indexes of the orthogonal pair of states s_0 and s_1. The value of $\bar{n}$ will always lie on the equator of the sphere, regardless of the orientation of the states s_0 and s_1, since s_0 and s_1 are an orthogonal pair. The direction cosine for each polarization-state is given by

$$\delta n_{\rm si} = \frac{\Delta n}{2} \cos \phi_{\rm si} = n_{\rm si} - \bar{n}; \qquad i = 0, 1, 2, 3. \tag{8}$$

Using the relationship $\cos^2 \phi_{s1} + \cos^2 \phi_{s2} + \cos^2 \phi_{s3} = 1$ for the direction cosines, the birefringence is expressed as

$$\Delta n = 2\sqrt{\delta n_{s1}^2 + \delta n_{s2}^2 + \delta n_{s3}^2}. \tag{9}$$

The effective index $n_{\rm eff}$ values of the two eigenstates can then be expressed as $n_{\rm eff}^{\rm fast} = \bar{n} - \Delta n/2$ and $n_{\rm eff}^{\rm slow} = \bar{n} + \Delta n/2$. Moreover, $\bar{n}$ is equivalent to measurements performed with unpolarized light, as in the study in [4]–[6]. Thus, both the longitudinal and transverse stresses in the FBG are fully characterized by this method.

A possible limitation of this method may be that the four-state, as presented here, calculates only the vector magnitude of the birefringence, so no information is available as the absolute orientation of the stress eigenstates due to the arbitrary orientation of the fiber. Because of this, we define the transverse-stress difference

$$\sigma_y - \sigma_x = \frac{\Delta n}{C_1 - C_2} \tag{10}$$

which is derived from (2) and (3). However, the relative orientation between two or more differently orientated strains can be found by comparing the direction cosines of each region.

III. Experimental Setup

To demonstrate the flexibility of the four-state method, we use two common interferometry methods to measure the phase-sensitive complex reflection spectrum of the FBG: LCI, and OFDR. While we note some of the merits and weaknesses of each technique, no attempt is made to directly compare the performance of each.

A commercial fiber-coupled polarization controller is placed at the output of the source in each system in order to set the desired polarization launch state. An interferogram is then collected at each of the four polarization-states. The typical time interval between each polarization measurement is about 1 min, which is the time it takes to reset the laser (OFDR) or the translation stage (LCI), save the digitized data, and move the polarization controller to the next polarization-state. This

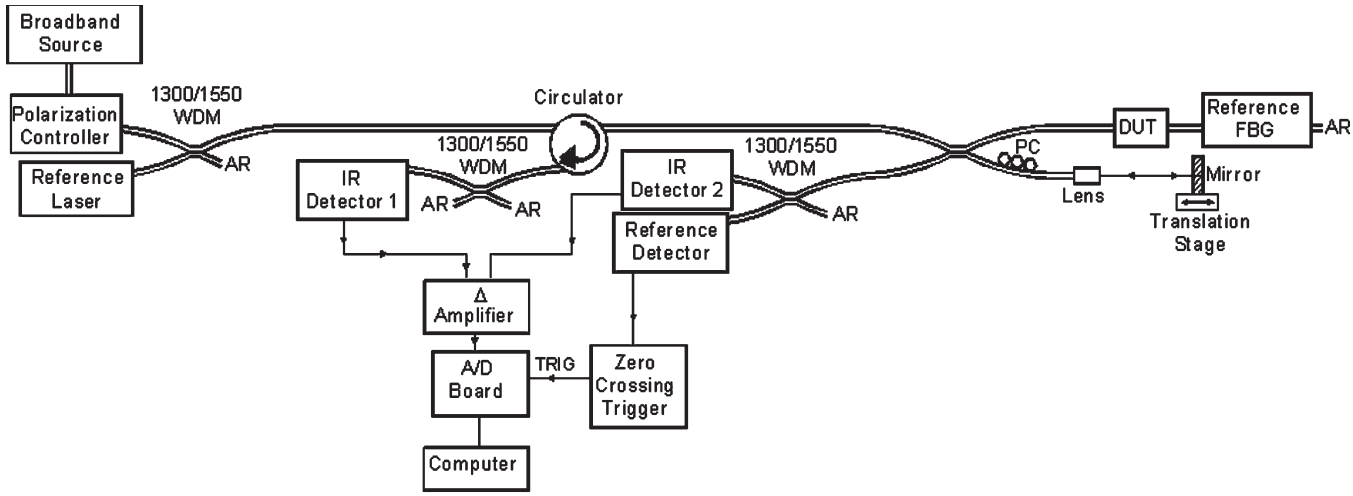

Fig. 4. Low-coherence measurement system. DUT: device under test. AR: antireflection. PC: polarization control, for matching the polarization-state of the two arms. WDM: wavelength-division multiplexer.

time is similar for both systems. Alternatively, it would possible to measure the four polarization-states simultaneously by illuminating the FBG with unpolarized light and then detecting with four separate detectors, each measuring the appropriate polarization-state. This would greatly increase the measurement speed to both systems and should be considered necessary for real-time monitoring of the sensor.

A. LCI System

LCI uses broadband illumination of the FBG. The FBG is placed in the test arm of a Michelson interferometer. Due to the low coherence of the source, interference occurs only when the optical path lengths of the test and reference arms are equal.

The impulse response of the FBG is measured with the fiber-optic Michelson LCI, as shown in Fig. 4. We have previously shown that the accurate high-resolution measurements of the dispersive and spectral properties of the optical components can be achieved with this measurement system [11]. The complex spectrum is found from the fast Fourier transform (FFT) of the measured impulse response. This measured spectrum must then be deconvolved with a measurement with the FBG replaced by a mirror in order to remove any system-dependent errors, such as spectral shape of the broadband source and dispersion. The system shows good long-term stability, so a new measurement of the empty system is required only when changes are made.

The FBG to be measured (device-under-test, DUT) is placed in one arm of the Michelson LCI along with a 1319-nm reference grating. The reference arm of the interferometer has a variable air path that is capable of scanning a total optical path distance of 1.4 m. The low-coherence illumination is provided by a commercial C+L band superfluorescent source with a 3-dB bandwidth of 85 nm centered at 1565 nm. The polarization launch states for the low-coherence light are set with a polarization controller. A 1319-nm Nd:YAG reference laser tracks the interferometer's total optical path difference as the reference arm mirror is translated. The reference grating provides a narrowband reflection of just the reference laser signal. The low-coherence signal is differentially detected and then digitized with a 16-bit A/D card. Triggering occurs at every zero crossing of the interference signal created by the reference laser, which sets the sample spacing to 659.5 nm. The signal-to-noise ratio is greater than 70 dB (20 Log of detector current), measured as the signal peak divided by the standard deviation of the noise.

The localized index changes in the FBG that are induced by external stress often result in a reflection spectrum with very fine spectral details. Such a spectrum will have a very long impulse response. When measuring these gratings with our interferometric system, we find it necessary to scan over a very long length to accurately capture the interferogram. Typical scan lengths are 2^{19} data points, or about 35 cm of scan mirror travel. Shorter scans can result in a spectrum that is distorted by the smoothing of these fine spectral features. Typical measurement time is between 5 and 12 s for each polarization-state, dependent on the scanning speed of the translation stage.

The spatial resolution of the calculated FBG index profile is inversely related to the bandwidth of the low-coherence source [7]. A spectral range from 1525 to 1610 nm gives a longitudinal spatial resolution for the FBG sensor of 10.2 μm in air.

B. OFDR System

OFDR illuminates the FBG with a narrow bandwidth tunable laser that is swept through its tuning range. A principal advantage of OFDR systems is their fast measurement times. Since the tunable laser contains the only moving parts and are often designed to tune swiftly, OFDR systems are typically faster when compared to LCI systems, which allows for averaging to reduce noise. OFDR systems have been shown to have lower inherent noise floors than LCI systems [12]. However, in practice, the noise advantage can be difficult to achieve. Deconvolution of the source spectrum from the measurement is nontrivial and is not done here. This leads to errors in the magnitude and phase of the measure spectrum. Moreover, inaccurate wavelength tracking can lead to excessive phase errors.

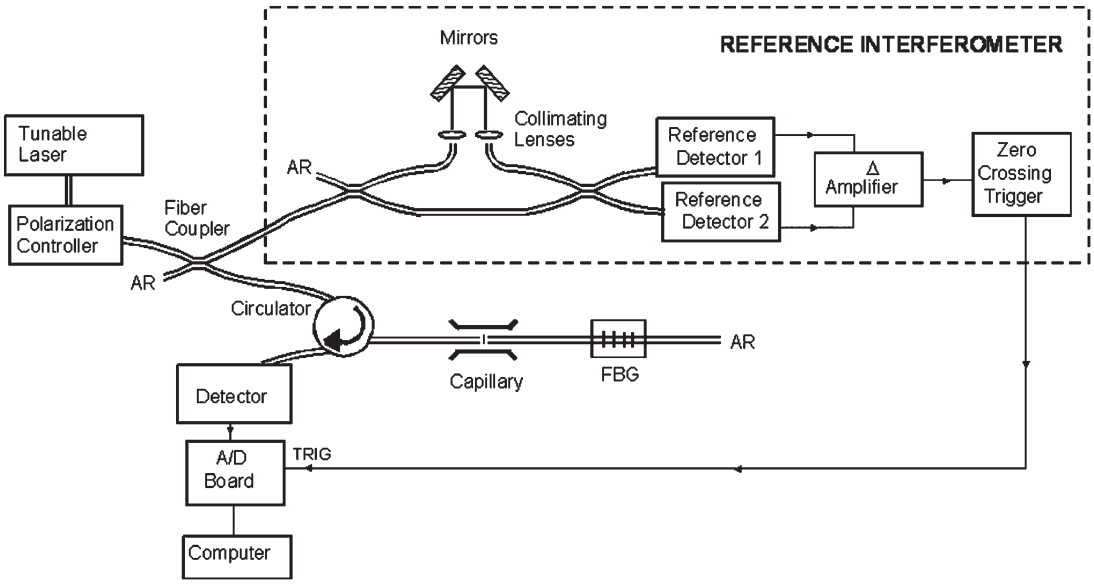

Fig. 5. OFDR measurement system. Measurement interferometer is a Fabry–Pérot configuration. An unbalanced Mach–Zender reference interferometer tracks the wavelength of the laser as it sweeps, triggering the A/D sampling in order to compensate for nonlinear tuning. The polarization controller sets the tunable laser light to the desired polarization launch state.

The flexibility and speed of the frequency-domain interferometry technique used allows for a simplified sensor interrogation when compared with the LCI system. Additionally, this method has the potential for real-time monitoring of the sensor, as well as being able to demultiplex a distributed sensor network.

The OFDR measurement system is shown in Fig. 5. The measurement interferometer is a Fabry–Pérot configuration, with the sensing FBG forming one end of the cavity and an air/glass interface of a butt coupling inside a capillary forming the other end. The distance between the butt-couple joint and the FBG is $d = 18$ cm, which forms a cavity with a free spectral range of 4.5 pm.

Tuning nonlinearity is corrected with an unbalanced Mach–Zender reference interferometer. The reference signal is differentially detected and used to trigger the A/D sampling at every zero crossing. The path imbalance used in the reference interferometer gives a sample spacing of about 0.5 pm, which oversamples the measurement Fabry–Pérot interferometer signal ten times per fringe. This signal is then digitized by a 16-bit A/D card.

The impulse response of the FBG is found from the inverse FFT at a delay equal to the time delay in the sensor cavity. The windowed impulse response is then Fourier transformed to produce the FBG's complex spectrum.

Measurement time is approximately 3 s for each polarization-state, dictated by the laser's tuning speed of 25 nm/s. Faster measurements are possible with other lasers. The spatial resolution of the calculated FBG index profile is 11.8 μm in air, given the laser's tuning range of 1511–1580 nm.

C. Fiber Loading Fixture

Transverse loads are applied to the FBG, with the fixture shown in Fig. 6, and is similar to that used in the study in [2] and [3]. With this fixture, a known compressive force can be applied to the FBG in a controlled manner by placing weights on top of the fixture. The test FBG and a support fiber are sandwiched between two thick polished-glass plates. The support fiber ensures that the plates are parallel, so that, the compressive force is always perpendicular to the plates.

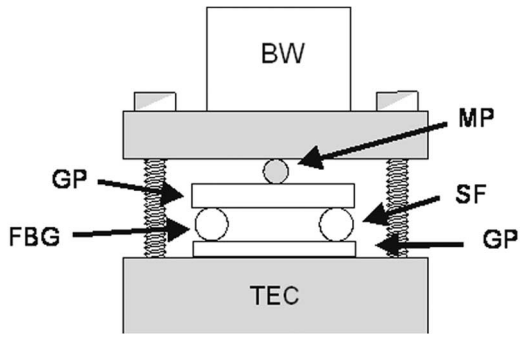

Fig. 6. Schematic of the fiber-loading fixture. SF: support fiber. GP: glass plate. MP: metal pin. BW: brass weight. TEC: thermoelectric cooler.

A metal pin is placed between the upper glass plate and the aluminum top plate and centered between the two fibers to prevent torsion of the load and to evenly distribute the load between the two fibers. In this configuration, the force applied to the FBG is $mg/2$; m is the applied mass, and g is the gravitational constant. Two screws are used to hold the top plate in place and keep it from rotating out of position when the weights are added. The screws are left loose so as not to add any compression. The weights are balanced directly above the pin so that the screws affect the load as little as possible. The jacket was stripped from both the FBG and the support fibers. This was done out of concern that permanent deformation of the soft jacket material caused by loading pressures might affect later measurements in an unpredictable manner.

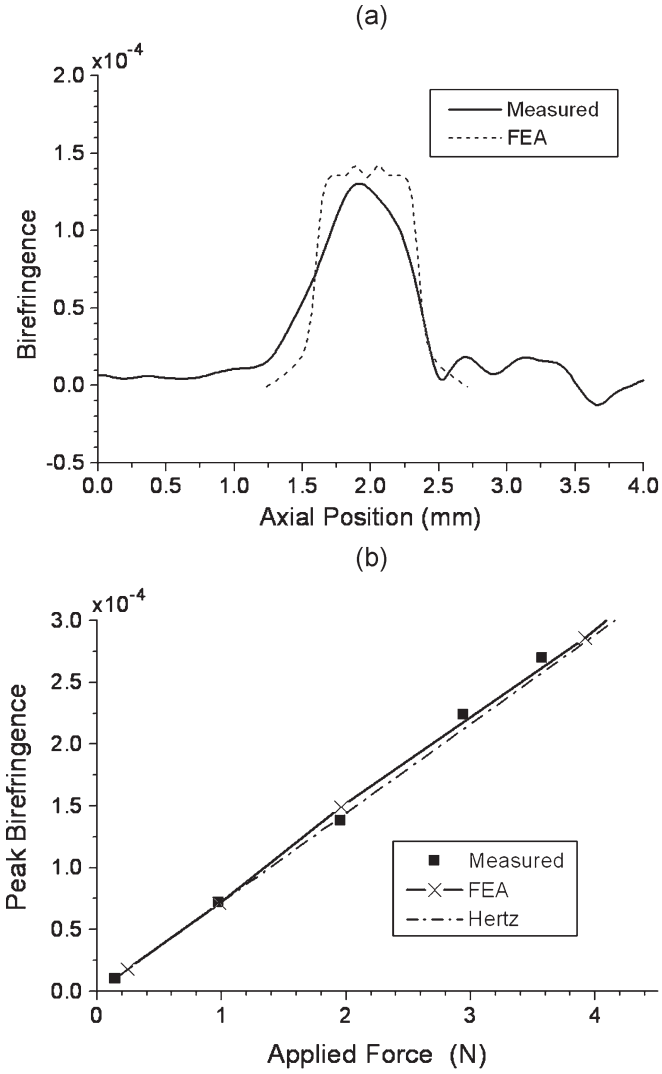

Fig. 7. (a) LCI measured and calculated birefringence in the core of the FBG near the location of the metal strip. (b) Peak value of the birefringence in plot (a) for several different applied forces. FEA: finite-element analysis.

IV. Results

A. Measurements With LCI

We used a 2.5-cm-long FBG written in a common non-PM single-mode fiber that had been previously hydrogen-loaded. The hydrogen loading was done to increase photosensitivity when writing the FBG. The FBG has a peak reflectivity of 15.5 dB at 1538.5 nm.

A 500-μm-wide aluminum strip was placed under the FBG in the loading fixture to produce a localized transverse stress. The FBG was measured with the low-coherence system, and the birefringence Δn was found with the layer-peeling and four-state algorithms (the results are plotted in Fig. 7). The peak birefringence agrees with the values predicted by the Hertz equations. We found the sensor to be very sensitive to even small applied loads, including the 15-g load placed by the unladen fixture.

A finite-element-analysis (FEA) model was used to predict and verify the measured transverse stress in the FBG. The fiber was modeled as a solid cylinder of fused silica. The cylinder was then placed under a localized compressive load by a metallic block of length L. The transverse-stress values were computed along the axis of the cylinder, simulating the stress in the core of the FBG sensor. The FEA stress was calculated for a 500-μm-wide block with the applied forces used in the measurement. There is good agreement between the measured birefringence and predicted by FEA and (2) and (3). The measured birefringence profile in Fig. 7(a) matches the FEA profile reasonably well in terms of overall width and height. The cause for the difference in shape is not fully understood but is most likely caused by improper coupling between the aluminum strip and the FBG.

Sensitivity is limited by the noise in the measurement system. Overall noise is estimated by the standard deviation of Δn in an unstressed section of the FBG. This is typically 5×10^{-6}. By (10), the minimum detectable stress is $\sigma_y - \sigma_x = 1.4\ \mathrm{N \cdot mm^{-2}}$.

B. Measurements With OFDR

The FBG used in the LCI measurements was no longer available; therefore, a different FBG was used for the sensing element in the OFDR system. The FBG used was 1.5 cm long with 11-dB peak reflectivity at 1538.5 nm, which is, again, written in a non-PM single-mode fiber. The localized transverse stress was produced by a 660-μm-wide aluminum strip. The FBG was measured with the OFDR system, and the birefringence Δn was found with the layer-peeling and four-state algorithms (the results are plotted in Fig. 8). Each measurement is the average of five sequential scans of the tunable laser.

The results were compared with another FEA that takes into account the wider strip. There is good agreement between the measured birefringence and that predicted by FEA. The measured birefringence profile in Fig. 8(a) matches the FEA profile reasonably well. The cause for the peaks at the edges is most likely improper coupling between the aluminum strip and the FBG. It appears as though the fiber is bending around the strip, causing a stress higher at the edges and lower in the center. This nonuniform loading could explain the apparent "noise" in the measured peak birefringence in Fig. 8(b).

The noise floor for Δn measured with the OFDR system, again as the standard deviation of an unstressed section, is better than 2×10^{-5} for a single-scan measurement, somewhat higher than for the LCI system. Averaging statistically reduces the noise by a factor of the square root of the number of samples taken. With five scans, the minimum sensitivity is similar to the LCI results, although still somewhat higher. Possible causes for the higher noise in the OFDR system could be the lower reflected power from the weaker FBG, loss at the butt-couple joint, or errors caused by the tunable laser previously discussed in Section III-B.

V. Temperature Effects

A common limitation of FBG sensors is that they are sensitive to both temperature changes and mechanical strain. Thermally induced index changes in the fiber can be difficult to

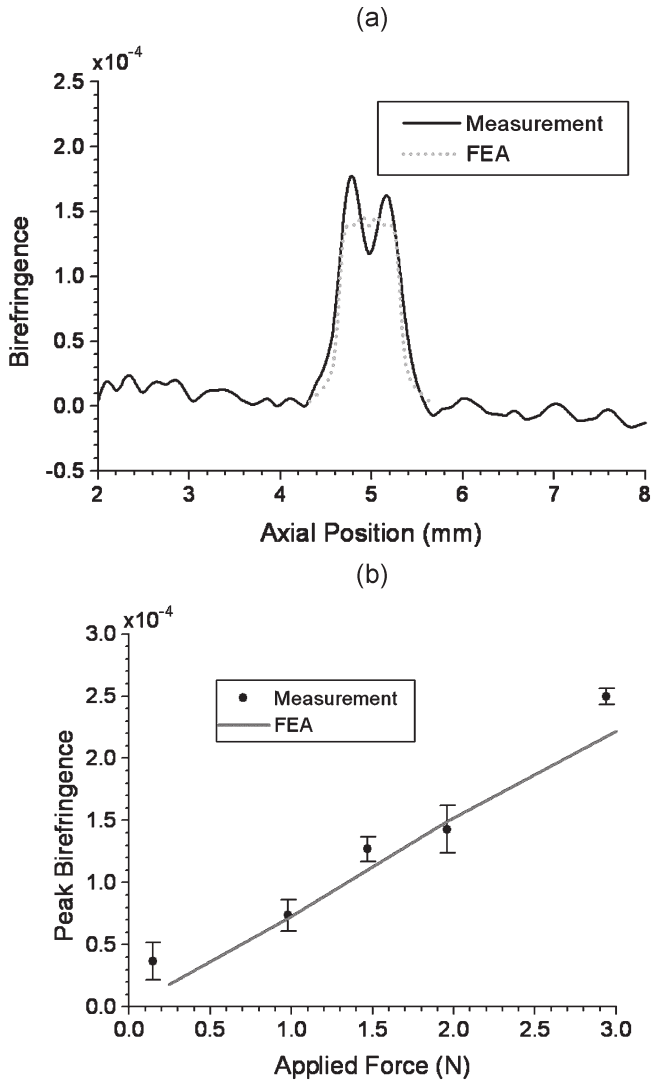

Fig. 8. (a) OFDR measured and calculated birefringence in the core of the FBG near the location of the localized strain created by the metal strip for a 2-N load. (b) Peak value of the birefringence in plot (a) as a function of applied force for several different applied forces. Points represent the average, and error bars represent the standard deviation (two sigma) of four independent measurements. FEA: finite-element analysis.

separate from mechanical strains. However, we show that this is less of an issue with high-resolution transverse stress when measured with the four-state method.

External environmental thermal loads have two overall effects on the refractive index. Increasing temperature increase the polarizability of the material, which raises the index. Increased temperature also causes the material to expand, which in turn reduces the refractive index while increasing the grating pitch Λ_B. For fused silica, which has a low coefficient of thermal expansion, this effect is weaker, and thus, the overall effect is an increase in refractive index with increasing temperature [13]. The response to temperature has been shown to be very linear over a broad temperature range of -200 °C–400 °C, allowing thermooptic effects to be described by a simple thermooptic coefficient dn/dT [13], [14]. Within the 1500–1600-nm wavelength range, dn/dT is 1.19×10^{-5} °C^{-1} [14], [15].

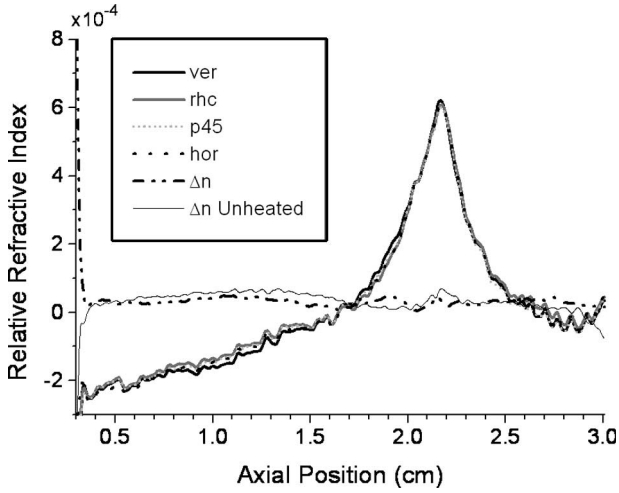

Fig. 9. Measured n_{eff} for the four polarization-states (ver $= 0°$, rhc $=$ right-hand circular, $p45 = +45°$, and hor $= 90°$) and calculated Δn with a localized 114-°C heat source. The four states are practically indistinguishable, and thus, the Δn is nominal despite the dramatic change seen in the individual states due to the applied heat.

A. Birefringence From Localized Heat Sources

To investigate the possible effects of thermal gradients on the birefringence, we used an additional FEA to predict the refractive index as a function of position in the FBG created by a point source of heat. The FBG was modeled as a solid cylinder of fused silica, which is 125 μm in diameter. For the properties of fused silica, the FEA model used thermal conductivity $= 1.38\ \text{W} \cdot \text{m}^{-1} \cdot \text{K}^{-1}$, specific heat $= 703\ \text{J} \cdot \text{kg}^{-1} \cdot \text{K}^{-1}$, and the density $= 2.203 \times 10^3\ \text{kg} \cdot \text{m}^{-3}$ [16]. Allowances were made for convective cooling of its surface in air at 22 °C, the average room temperature in which the experiment was performed. This was done to provide insight into the response of the fiber to an impulse of heat and can be regarded as a worst case scenario.

We found that, with the exception of the most extreme case of a very hot localized heat source (more than 100 °C above the ambient temperature), thermal diffusion will cause gradients to be negligible over small scales such as the diameter of the fiber. In real applications, it is likely that the large thermal mass of the host material will have a greater influence on temperature distribution and will smooth out any large fluctuations. Therefore, both eigenstates should see the same thermally induced change in refractive index. Thus, due to the differential nature of the birefringence measurement, this detection method should not be susceptible to thermal effects.

A localized thermal load was applied to the FBG by a heated knife-edge. The blade of the knife-edge is perpendicular to the fiber and is meant to approximate a point heat source. The knife-edge was heated to 114 °C, which was actively monitored and controlled with a thermocouple near the tip and a commercial temperature controller. The FBG is mounted suspended in air to isolate it from heat-conducting surfaces that would cause unexpected results. Measurements were then made with both the LCI and OFDR systems. Both systems show similar results. Fig. 9 shows the measured n_{eff} for the four polarization launch states, as well as the calculated Δn. Despite

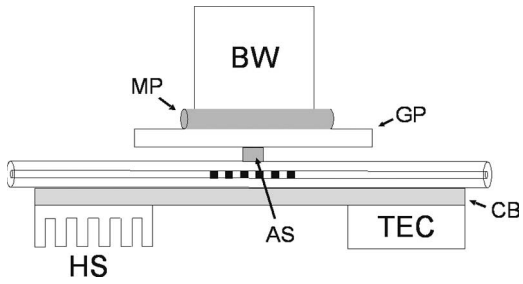

Fig. 10. Modified loading setup to induce thermal gradients across the FBG. The TEC heats one end of the CB, while the heat sink maintains the other end at room temperature. The rest of the loading setup is the same, as in Fig. 6, but shown from a side view instead. For clarity, the screws and support fiber are not shown. As before, weight is applied to a small metal strip to produce localized transverse stress in the FBG in a controlled manner. HS: heat sink. BW: brass weight. GP: glass plate. AS: 660-μm aluminum strip. MP: metal pin.

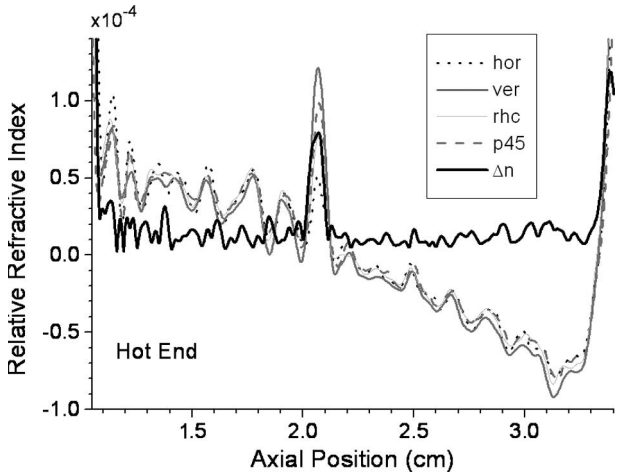

Fig. 11. Measured index profile of the four polarization-states and the calculated birefringence for a 0.6-°C · mm^{-1} temperature gradient and 0.3-N applied load.

the very large change in n_{eff} seen for the different launch states, Δn does not deviate much from its value for the unheated state.

B. Effects of Thermal Gradients on Transverse Stress

We repeated the measurements of transverse stress in the presence of a thermal gradient. To produce the gradient, we modified the loading fixture as in Fig. 10. A long copper bar (CB) with dimensions $1 \times 25 \times 100$ mm replaces the bottom glass plate in Fig. 6. The modified fixture creates a linear temperature gradient by placing a heat source (thermoelectric cooler, TEC) and a heat sink at opposite ends of a CB [17]. Measurements of transverse stress were carried out as before with several different TEC temperatures using the OFDR system. Measurements were not repeated with the LCI system; however, it is assumed that it should yield similar results.

The measured n_{eff} for each of the four polarization-states and the calculated Δn are plotted in Fig. 11 for a 0.3-N load and a 0.6-°C · mm^{-1} temperature gradient. The n_{eff} of the four states shows a linear increase from right to left in response to the increasing temperature.

The peak birefringence was measured for a 0.98- and 2.55-N applied load for several different temperature gradients

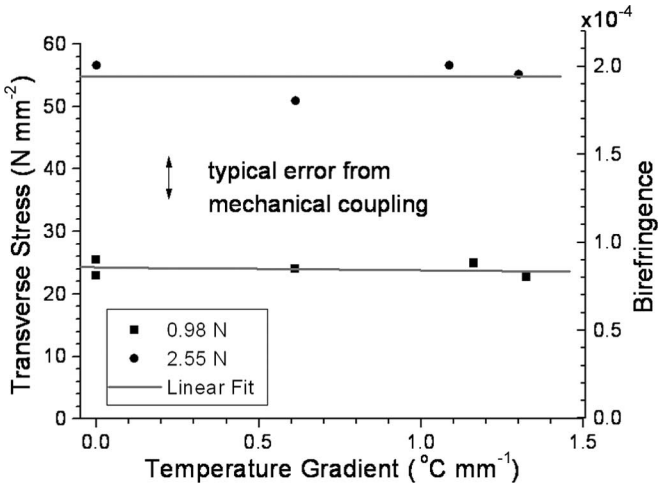

Fig. 12. Peak value of the measured birefringence for two different loads at several temperature gradients along the 15-mm-long FBG. Uncertainty bar shows typical error (as shown in Fig. 8).

and is plotted in Fig. 12. For each set of load results, a linear fit to Δn was performed. The slope of the fit for the 0.98- and 2.55-N loads is nominally zero in both cases. The measured peak birefringence is unaffected by the temperature gradient, as predicted by the FEA simulations.

VI. Conclusion

We have demonstrated an accurate transverse-stress-sensing method using a four-state polarization analysis that yields high spatial resolution and does not require PM optics. Both the transverse and longitudinal stresses were measured by this method, allowing for the complete characterization of the local state of stress. The four-state polarization detection method has also been shown to be insensitive to thermal effects.

The method presented could be applied as a periodic test to traditional FBG sensors, as described in [1] and [2], to ensure that highly localized strains are not affecting and degrading the sensors' performance. The high spatial resolution achieved by this method makes the sensor ideal for small-scale applications requiring high resolution, such as the testing and monitoring of composite materials for internal delamination failures.

References

[1] E. Udd, "An overview of fiber optic sensors," *Rev. Sci. Instrum.*, vol. 66, no. 8, pp. 4015–4030, Aug. 1995.

[2] C. M. Lawrence, D. V. Nelson, E. Udd, and T. Bennett, "A fiber optic sensor for transverse strain measurement," *Exp. Mech.*, vol. 39, no. 3, pp. 202–209, Sep. 1999.

[3] R. B. Wagreich, E. A. Altia, H. Singh, and J. S. Sirkis, "Effects of diametric load on fibre Bragg gratings in low birefringence fibre," *Electron. Lett.*, vol. 32, no. 13, pp. 1223–1224, Jun. 1996.

[4] P. Giaccari, G. R. Dunkel, L. Humbert, J. Botsis, H. G. Limberger, and R. P. Salathe, "On a direct determination of non-uniform internal strain fields using fibre Bragg gratings," *Smart Mater. Struct.*, vol. 14, no. 1, pp. 127–136, Feb. 2005.

[5] X. Chapeleau, D. Leduc, C. Lupi, F. López-Gejo, M. Douay, R. Le Ny, and C. Boisrobert, "Local characterization of fiber-Bragg gratings through combined use of low-coherence interferometry and a layer-peeling algorithm," *Appl. Opt.*, vol. 45, no. 4, pp. 728–735, Feb. 2006.

[6] E. Udd, "Fiber grating sensors for structural health monitoring of aerospace structures," *Proc. SPIE*, vol. 6167, p. 61 670C-1, Mar. 2006.

[7] J. Skaar, L. Wang, and T. Erdogan, "On the synthesis of fiber Bragg gratings by layer peeling," *IEEE J. Quantum Electron.*, vol. 37, no. 2, pp. 165–173, Feb. 2001.
[8] R. M. Craig, S. L. Gilbert, and P. D. Hale, "High-resolution, nonmechanical approach to polarization-dependent transmission measurements," *J. Lightw. Technol.*, vol. 16, no. 7, pp. 1285–1294, Jul. 1998.
[9] P. A. Williams, "Modulation phase-shift measurement of PMD using only four launched polarisation states: A new algorithm," *Electron. Lett.*, vol. 35, no. 18, pp. 1578–1579, Sep. 1999.
[10] W. C. Swann, S. D. Dyer, and R. M. Craig, "Four-state measurement method for polarization dependent wavelength shift," in *Proc. SOFM*, Boulder, CO, 2002, pp. 125–128. NIST Spec. Publ. 988.
[11] S. D. Dyer, R. J. Espejo, and P. A. Williams, "High-resolution group delay measurements of a hydrogen cyanide gas cell using low-coherence interferometry," in *Proc. SOFM*, Boulder, CO, 2002, pp. 45–48. NIST Spec. Publ. 988.
[12] R. Leitgeb, C. K. Hitzenberger, and A. F. Fercher, "Performance of Fourier domain vs. time domain optical coherence tomography," *Opt. Express*, vol. 11, no. 18, pp. 889–894, Apr. 2003.
[13] J. Simmons, *Optical Materials*. San Diego, CA: Academic, 2000, pp. 108–110.
[14] T. Toyoda and M. Yabe, "The temperature dependence of the refractive indices of fused silica and crystal quartz," *J. Phys. D, Appl. Phys.*, vol. 16, no. 5, pp. L97–L100, May 1983.
[15] W. Driscoll, *Handbook of Optics*. New York: McGraw-Hill, 1978, p. 174.
[16] G. W. Morey, *The Properties of Glass*. New York: Reinhold, 1954, ch. 8.
[17] J. Lauzon, S. Thibault, J. Martin, and F. Ouellette, "Implementation and characterization of fiber Bragg gratings linearly chirped by a temperature gradient," *Opt. Lett.*, vol. 19, no. 23, pp. 2027–2029, Dec. 1994.

R. Joseph Espejo received the B.S. degree in physics from the University of Colorado, Boulder, in 1999, where he is currently working toward the Ph.D. degree in electrical engineering.

He is currently a Research Assistant at the National Institute of Standards and Technology, Boulder. His research interests include interferometry and fiber Bragg grating for metrology and sensing applications.

Shellee D. Dyer received the Ph.D. degree in electrical engineering from the University of Utah, Salt Lake City, in 1996.

She then joined the National Institute of Standards and Technology, Boulder, CO, as a National Research Council Postdoctoral Fellow, where she is currently a Senior Electronics Engineer in the Optoelectronics Division. Her current research interests include optical coherence tomography, dispersion metrology, spectral-domain interferometry, biophotonics, and optical fiber sensors.